7

Corrosive Effects of Chlorides on Metals

Fong-Yuan Ma
Department of Marine Engineering, NTOU
Republic of China (Taiwan)

1. Introduction

1.1 Introduce of pitting corrosion

Alloying metallic elements added during the making of the steel increase corrosion resistance, hardness, or strength. The metals used most commonly as alloying elements in stainless steel include chromium, nickel, and molybdenum. Due to the alloy contains different, in general, stainless steels are separated the grouped into martensitic stainless steels, ferritic stainless steels, austenitic stainless steels, duplex (ferritic-austenitic) stainless steels and precipitation-hardening stainless steels.

Since stainless steel resists corrosion, maintains its strength at high temperatures, and is easily maintained, it is widely used in items such as automotive, propulsion shaft for high speed craft and food processing products, as well as medical and health equipment. The displacement of a high-speed craft is lighter than the displacement of a conventional ship. This displacement aspect is the essential parameter to obtain fast and competitive sea transportations. High-speed craft allows for the use of non-conventional shipbuilding materials provided that a safety standard at least equivalent to that of a conventional ship is achieved. The chapter will describe the corrosion characteristics stainless steels for SUS630,

Stainless steels are used in countless diverse applications for their corrosion resistance. Although stainless steels have extremely good general resistance, stainless steels are nevertheless susceptible to pitting corrosion. This localized dissolution of an oxide-covered metal in specific aggressive environments is one of the most common and catastrophic causes of failure of metallic structures. The pitting process has been described as random, sporadic and stochastic and the prediction of the time and location of events remains extremely difficult. Many contested models of pitting corrosion exist, but one undisputed aspect is that manganese sulphide inclusions play a critical role.

Pitting corrosion is localized accelerated dissolution of metal that occurs as a result of a breakdown of the otherwise protective passive film on metal surface. The phenomenology of pitting corrosion is discussed, including the effects of alloy composition, environment, potential, and temperature. Those have focused on various stages of pitting process, including breakdown of the passive film, metastable pitting, and pit growth. The mechanism of pitting corrosion is similar to that of Crevice corrosion: dissolution of the passivating film and gradual acidification of the electrolyte caused by its insufficient aeration.

Within the pits, an extremely corrosive micro-environment tends to be established, which may bear little resemblance to the bulk corrosive environment. For example, in the pitting of

stainless steels in water containing chloride, a micro-environment essentially representing hydrochloric acid may be established within the pits. The pH within the pits tends to be lowered significantly, together with an increase in chloride ion concentration, as a result of the electrochemical pitting mechanism reactions in such systems. Pitting is often found in situations where resistance against general corrosion is conferred by passive surface films. A localized pitting attack is found where these passive films have broken down. Pitting attack induced by microbial activity, such as sulfate reducing bacteria also deserves special mention. Most pitting corrosion in stainless alloys occurs in neutral-to-acid solutions with chloride or ions containing chlorine.

The detection and meaningful monitoring of pitting corrosion usually represents a major challenge. Monitoring pitting corrosion can be further complicated by a distinction between the initiation and propagation phases of pitting processes. The highly sensitive electrochemical noise technique may provide early warming of imminent damage by characteristic in the pit initiation phase. Pitting failures can occur unexpectedly, and with minimal overall metal loss.

Furthermore, the pits may be hidden under surface deposits, and/or corrosion products. A small, narrow pit with minimal overall metal loss can lead to the failure of an entire engineering system. Pitting corrosion, which, for example, is almost a common denominator of all types of localized corrosion attack, may assume different shapes. Corrosion of metals and alloys by pitting constitutes one of the very major failure mechanisms. Pits cause failure through perforation and engender stress corrosion cracks and the life cycle of stainless alloy will decrease.

2. Pitting corrosion phenomenon

The pits often appear to be rather small at the surface, but may have larger cross-section areas deeper inside the metal. Since the attack is small at the surface and may be covered by corrosion products, a pitting attack often remains undiscovered until it causes perforation and leakage. The experimental evaluation of the parameters of a general stochastic model for the initiation of pitting corrosion on stainless steels is described. The variation of these parameters with experimental conditions is used in the development of a microscopic model. A microscopic model which accords with the observed behavior attributes the initiation of pitting corrosion to the production and persistence of gradients of acidity and electrode potential on the scale of the surface roughness of the metal. The observed fluctuations are related to fluctuations in the hydrodynamic boundary layer thickness. A pit becomes stable when it exceeds a critical depth related to the surface roughness.

2.1 Stainless steel metal

In 1913, English metallurgist Harry Brearly, working on a project to improve rifle barrels, accidentally discovered that adding chromium to low carbon steel gives it stain resistance. In addition to iron, carbon, and chromium, modern stainless steel may also contain other elements, such as nickel, niobium, molybdenum, and titanium. Nickel, molybdenum, niobium, and chromium enhance the corrosion resistance of stainless steel. It is the addition of a minimum of 12% chromium to the steel that makes it resist rust, or stain 'less' than other types of steel.

According to the MIL HDBK-73S and Japanese Industry Standard (JIS), there are different stainless steels grades with different corrosion resistance and mechanical properties:

a. Stainless Steel grades 200 Series

This group of alloys is similar to the more common 300 Series alloys described below as they are non-magnetic and have an austenitic structure. The basic Stainless Steel Grades 200 alloy contains 17% chromium, 4% nickel and 7% manganese. These alloys are, however, not immune to attack and are very susceptible to concentration cell corrosion and pitting corrosion attack. When corrosion starts they usually corrode rapidly and non-uniformly. In seawater immersion, the incubation time for these alloys is in the range of 1 to 3 months with some of the Nitronic grades having incubation times of up to 1 year.

b. Stainless Steel Grades 300 Series

This group of alloys are non-magnetic and have an austenitic structure. The basic Stainless Steel Grades 300 alloy contains 18% chromium and 8% nickel. These alloys are subject to crevice corrosion and pitting corrosion. They have a range of incubation times in seawater ranging from essentially zero in the case of the free machining grades, such as Type 303, to 6 months to 1 year for the best alloys, such as Type 316. They have been widely used in facilities with mixed results. If used in an application where chloride levels are low or where concentration cell corrosion has been prevented through design, they are likely to perform well. When chloride levels are high and where concentration cells can occur, the performance of these alloys is often poor. They must always be selected with care for a specific application and the effect of potential non-uniform attack on system performance must be addressed.

c. Stainless Steel Grades 400 Series

This group of alloys are magnetic and have a martensitic structure. The basic alloy contains 11% chromium and 1% manganese. These Stainless Steel Grades alloys can be hardened by heat treatment but have poor resistance to corrosion. They are subject to both uniform and non-uniform attack in seawater. The incubation time for non-uniform attack in chloride containing environments is very short, often only hours or a few days. Unless protected, using these Stainless Steel Grades in sea water or other environments where they are susceptible to corrosion is not recommended.

d. Stainless Steel Grades 600 Series

This series of stainless steels grade is commonly referred to as Precipitation Hardening stainless steels. These steels can be heat treated to high strength levels. They are subject to crevice corrosion and pitting in chloride containing environments and are also subject to stress corrosion cracking and hydrogen embrittlement. The incubation time for crevice corrosion and pitting in seawater is relatively short, often only a few days. The incubation time for stress corrosion cracking can be very short, sometimes measured in hours.

The use of this Stainless Steel Grade in chloride containing environments is not normally recommended unless they are carefully selected, their heat treatment is carefully specified and controlled, and the effect of pitting and crevice corrosion is properly addressed.

2.2 Principle of pitting corrosion

Pitting corrosion is an electrochemical oxidation-reduction process, which occurs within localized deeps on the surface of metals coated with a passive film.

Anodic reactions inside the pit:

$$Fe = Fe^{2+} + 2e^{-} \text{ (dissolution of iron)}$$

The electrons given up by the anode flow to the cathode where they are discharged in the cathodic reaction:

$$1/2O_2 + H_2O + 2e^{-} = 2(OH^{-})$$

As a result of these reactions the electrolyte enclosed in the pit gains positive electrical charge in contrast to the electrolyte surrounding the pit, which becomes negatively charged.

The positively charged pit attracts negative ions of chlorine Cl^{-} increasing acidity of the electrolyte according to the reaction:

$$FeCl_2 + 2H_2O = Fe(OH)_2 + 2HCl$$

pH of the electrolyte inside the pit decreases from 6 to 2-3, which causes further acceleration of corrosion process.

Large ratio between the anode and cathode areas favors increase of the corrosion rate. Corrosion products ($Fe(OH)_3$) form around the pit resulting in further separation of its electrolyte.

2.3 Stages of pitting corrosion

Pitting corrosion is treated as a time-dependent stochastic damage process characterized by an exponential or logarithmic pit growth. Data from propulsion shaft for high-speed craft is used to simulate the sample functions of pit growth on metal surfaces. Perforation occurs when the deepest pit extends through the thickness of the propulsion shaft. Because the growth of the deepest pit is of stochastic nature, the time-to-perforation is modeled as a random variable that can be characterized by a suitable reliability model. It is assumed that corrosion will occur at multiple pits on both sides of the rivet deeps and will cause multiple fatigue cracks. Therefore, system failure could occur due to the linkage between any two neighboring cracks.

2.3.1 Pit initiation

An initial pit may form on the surface covered by a passive oxide film as a result of the following:

a. Mechanical damage of the passive film was caused by scratches. Anodic reaction starts on the metal surface exposed to the electrolyte. The passivity surrounding surface is act as the cathode.
b. Particles of a second phase emerging on the metal surface. These particles precipitating along the grains boundaries may function as local anodes causing localized galvanic corrosion and formation of initial pits.
c. Localized stresses in form of dislocations emerging on the surface may become anodes and initiate pits.
d. Non-homogeneous environment may dissolve the passive film at certain locations where initial pits form.

2.3.2 Pitting growth

In presence of chloride ions pits are growing by autocatalytic mechanism. Pitting corrosion of a stainless steel is illustrated in the Figure 1. The actual pitting corrosion phenomenon is shown on propeller shaft of high speed craft, and the pit depth was measured with dial gauge as shown in Figure 2.

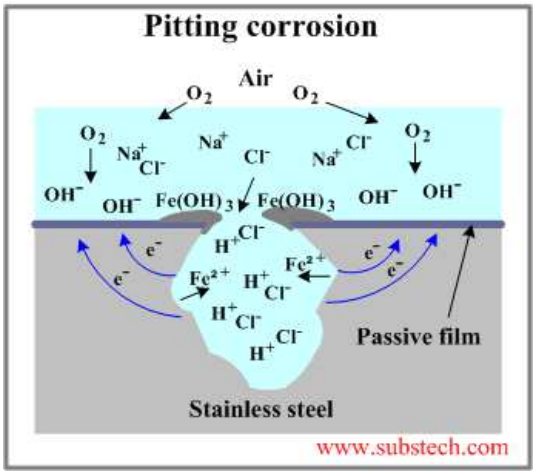

Fig. 1. Pitting corrosion deep growth

Fig. 2. Measuring depth of pitting deep

2.3.3 Transition from pitting to fatigue crack nucleation

The third stage is the transition from pit growth to fatigue crack nucleation, where mechanical effects such as the stress intensity factor come into play. The nucleation of the corrosion crack is essentially a competition between the processes of pit growth and crack growth. Two criteria are used to describe the transition process.

2.3.4 Short crack growth

The short crack growth stage involves chemical and microstructural factors and their interactions. Although much research has been done in this area, it has been difficult to derive an explicit formula for short crack growth, especially in corrosive environment. For computational simplicity, a probabilistic power law model is presented here to describe the relationship between the stress intensity factor and the growth rate. In this method, an empirically based probabilistic relationship is used to model the corrosion short crack growth.

2.3.5 Transition from short crack growth to long crack growth

Experimental and analytical approaches have been proposed to determine the transition size from short crack growth to long crack growth.

2.3.6 Long crack growth

The widely used Paris Law may be used in this stage to estimate the time for long crack growth.

2.3.7 Crack coalescence

The linkage between any two neighboring cracks is considered to be the failure criterion at this stage.

2.4 Pitting corrosion behavior

Corrosion of metals and alloys by pitting constitutes one of the very major failure mechanisms. Pits cause failure through perforation and engender stress corrosion cracks. Pitting is a failure mode common to very many metals. It is generally associated with particular anions in solution, notably the chloride ion. The origin of pitting is small. Pits are nucleated at the microscopic scale and below. Detection of the earliest stages of pitting requires techniques that measure tiny events.

Stainless steels are used in countless diverse applications for their corrosion resistance. Although stainless steels have extremely good general resistance, stainless steels are nevertheless susceptible to pitting corrosion. This localized dissolution of an oxide-covered metal in specific aggressive environments is one of the most common and catastrophic causes of failure of metallic structures. The pitting process has been described as random, sporadic and stochastic and the prediction of the time and location of events remains extremely difficult. Many contested models of pitting corrosion exist, but one undisputed aspect is that manganese sulphide inclusions play a critical role.

The chromium in the steel combines with oxygen in the atmosphere to form a thin, invisible layer of chrome-containing oxide, called the passive film. The sizes of chromium atoms and their oxides are similar, so they pack neatly together on the surface of the metal, forming a stable layer only a few atoms thick. If the metal is cut or scratched and the passive film is disrupted, more oxide will quickly form and recover the exposed surface, protecting it from oxidative corrosion.

The passive film requires oxygen to self-repair, so stainless steels have poor corrosion resistance in low-oxygen and poor circulation environments. In seawater, chlorides from the

salt will attack and destroy the passive film more quickly than it can be repaired in a low oxygen environment.

Some metals show preferential sites of pit nucleation with metallurgical microstructural and microcompositional features defining the susceptibility. However, this is not the phenomenological origin of pitting per se, since site specificity is characteristic only of some metals. A discussion is presented of mechanisms of nucleation; it is shown that the events are microscopically violent. The ability of a nucleated event to survive a series of stages that it must go through in order to achieve stability is discussed. Nucleated pits that do not propagate must repassivate. However, there are several states of propagation, each with a finite survival probability. Several variables contribute to this survival probability.

2.5 Electron fractography of fatigue fracture with pitting corrosion

The evolution of corrosion pits on stainless steel immersed in chloride solution occurs in three distinct stages: nucleation, metastable growth and stable growth. A microcrack generated by pitting corrosion, forms the initial origin for fatigue fracture. But in fact, fatigue failure is not certainly caused at the deepest interior pitting deep. Owing to the different shape of interior pitting deeps as shown in Figure 3, some of them are hard to start or to continue the crack propagation and play as a role of crack arrester, as shown in Figure 4. If the fracture is caused by the pitting deep as an inclusion, then continuous plastic deformation can be found around the pitting deep. The dimples are generally equalized by overloaded tension, and elongated by shear or tearing, as shown in Figure 5 and Figure 6.

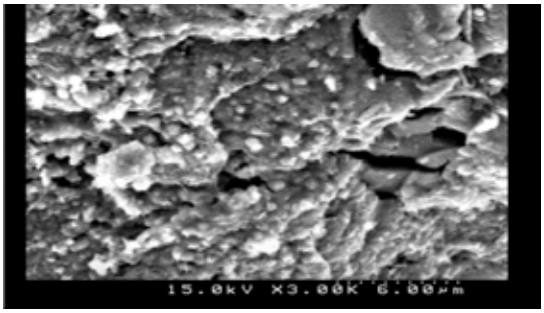

Fig. 3. Interior pitting deep

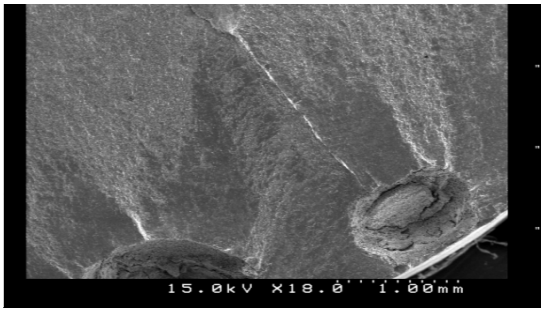

Fig. 4. Fatigue failure arrester at interior pitting deep

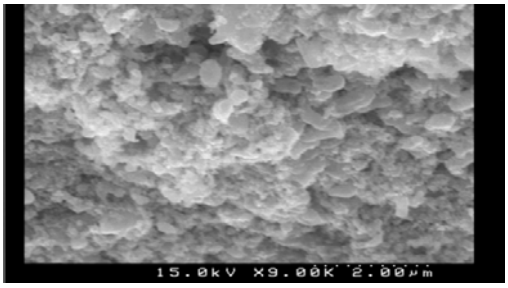

Fig. 5. Equalized dimples around interior pitting deep

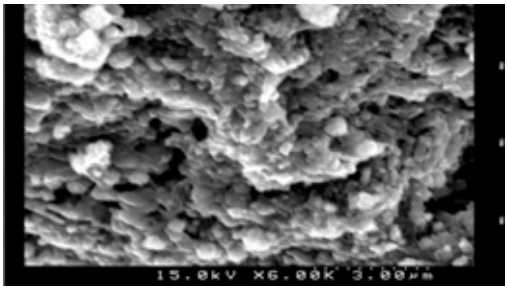

Fig. 6. Elongated dimples around interior pitting deep

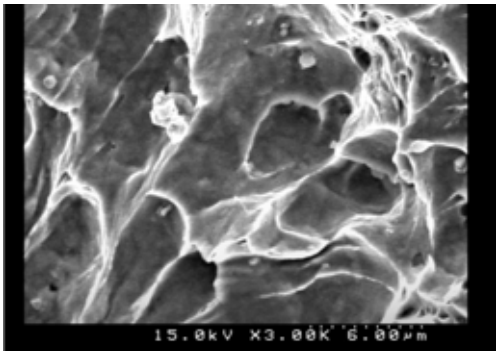

Fig. 7. Typical cleavage fractures in fracture area (3000 times)

The features of cleavage failure can be seen by flat fractography as shown in Figure 7 and Figure 8 with 3000 and 1000 times Scanning Electron Microscopy (SEM) respectively. Cleavage failure occurs by separation along crystallographic planes. This transgranular fracture is categorized to be the brittle fracture in the fracture area. There are several features can be identified to be cleavage, namely, herringbone, tongues and river stream. Figure 9 and Figure 10 show the microscopic fractographics of river stream and tongue patterns, which have seen in the study.

At grain boundaries the fracture plane or cleavage plane changes because of the differences of crystallographic orientations. Cleavages are not only associated with transgranular fracture, but also with brittle particles as shown in Figure 11 and Figure 12 respectively.

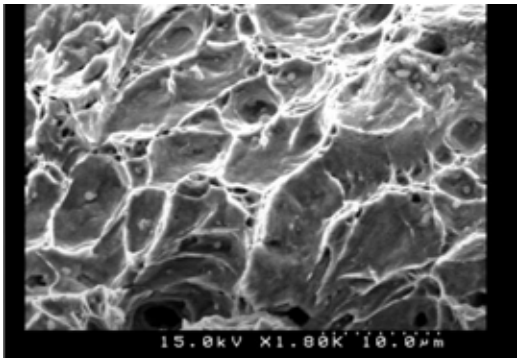

Fig. 8. Typical cleavage fractures in fracture area (1000 times)

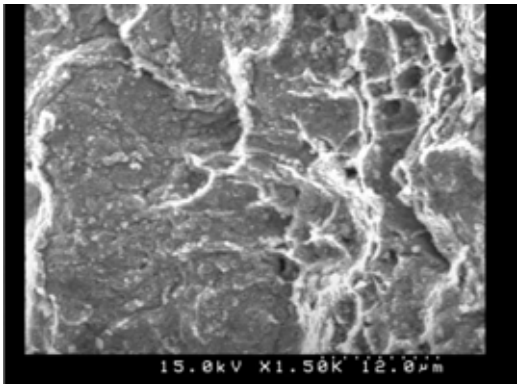

Fig. 9. River pattern in fatigue propagation area (1500 times)

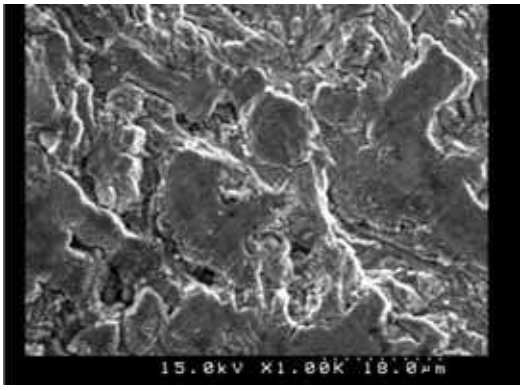

Fig. 10. Tongue pattern in fatigue propagation area (1000 times)

Some metals can fail in brittle manner, but do not cleave. These fractures are identified as quasi-cleavage. They are similar to cleavage but their features are usually fairly flat and smaller, as shown in Figure 13 and Figure 14.

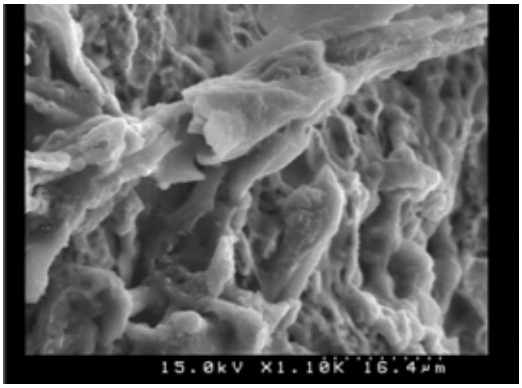

Fig. 11. Cleavage with transgranular fracture in fatigue propagation area

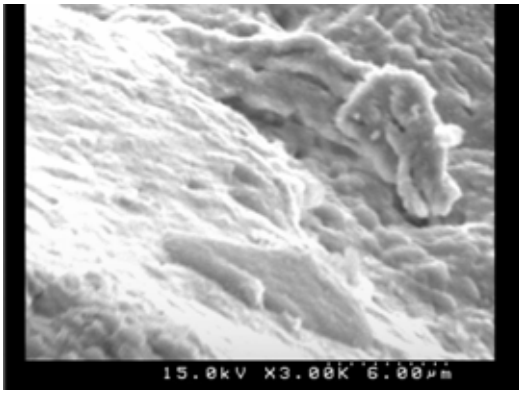

Fig. 12. Cleavage with brittle particles in fracture area

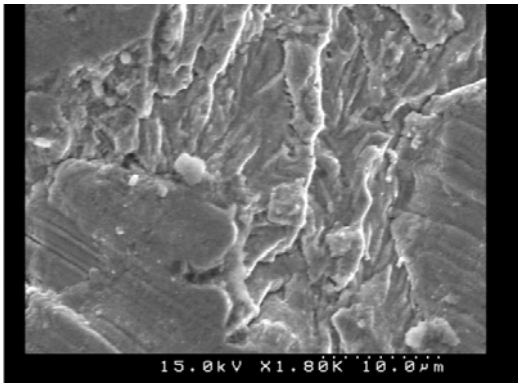

Fig. 13. Quasi-cleavage in fracture area (I)

Also the intergranular fracture can occur by a number of causes, but it is generally possible to be identified fractographically by the features of grain contours, grain boundaries and

triple points. Examples of this kind in tergranular fractures are tree pattern fracture and sub-crack caused by the interior pitting deeps, as shown as Figure 15 and Figure 16.

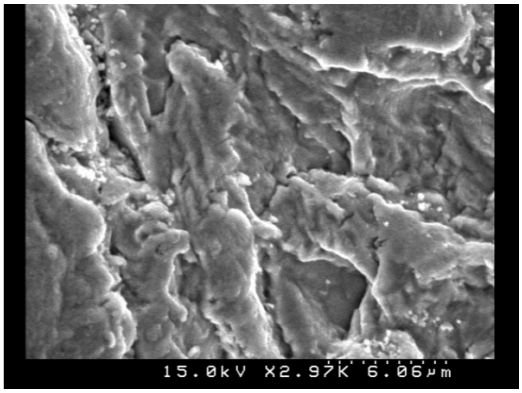

Fig. 14. Quasi-cleavage in fracture area (II)

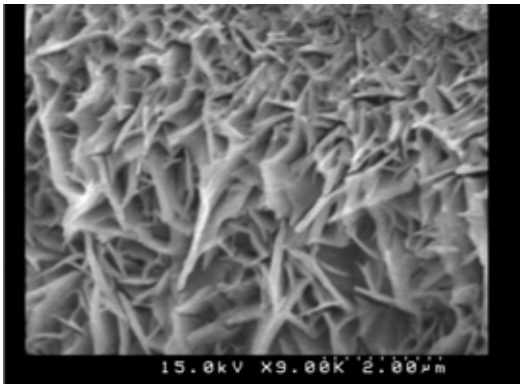

Fig. 15. Tree pattern fracture caused by interior pitting deep

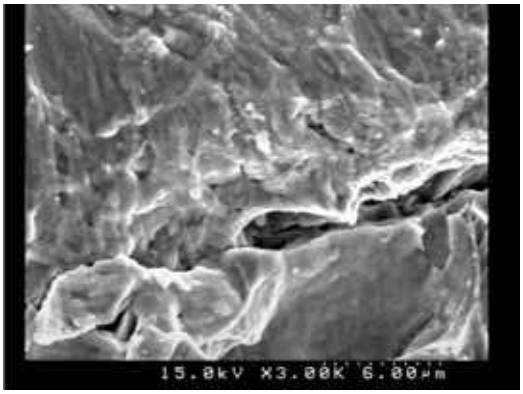

Fig. 16. Sub-crack caused by interior pitting deep

3. Initial pitting deep and pitting corrosion behavior

Pitting corrosion is a localized form of corrosion by which cavities or deeps are produced in the material. Pitting is considered to be more dangerous than uniform corrosion damage because it is more difficult to detect, predict and design against. Corrosion products often cover the pits. A small, narrow pit with minimal overall metal loss can lead to the failure of an entire engineering system.

3.1 Corrosion pit shapes

Pitting corrosion forms on passive metals and alloys like stainless steel when the ultra-thin passive film is chemically or mechanically damaged and does not immediately re-passivity. The resulting pits can become wide and shallow or narrow and deep which can rapidly perforate the wall thickness of a metal.

3.1.1 Pitting shape by ASTM

Pitting corrosion can produce pits with their mouth open or covered with a semi-permeable membrane of corrosion products. Pits can be either hemispherical or cup-shaped. In some cases they are flat-walled, revealing the crystal structure of the metal, or they may have a completely irregular shape. Pitting corrosion occurs when discrete areas of a material undergo rapid attack while most of the adjacent surface remains virtually unaffected.

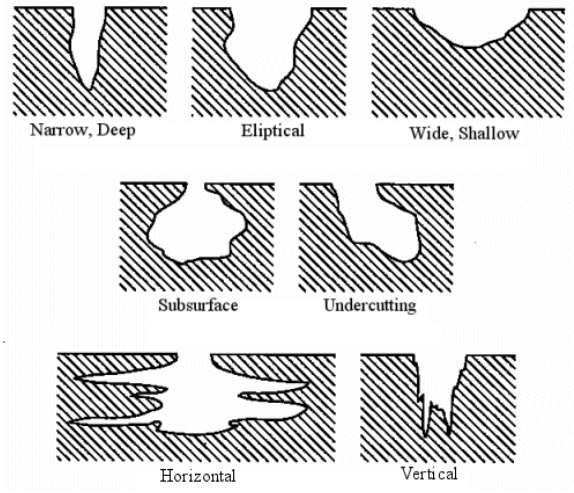

Fig. 17. ASTM-G46 has a standard visual chart for rating of pitting corrosion (http://www.corrosionclinic.com)

3.1.2 Experiment pitting shape

Localized chemical or mechanical damage to the protective oxide film; water chemistry factors which can cause breakdown of a passive film are acidity, low dissolved oxygen concentrations and high concentrations of chloride in seawater. The actual pitting shape was investigated by Scanning Electron Microscopy shown as Figure 18 and Figure 19.

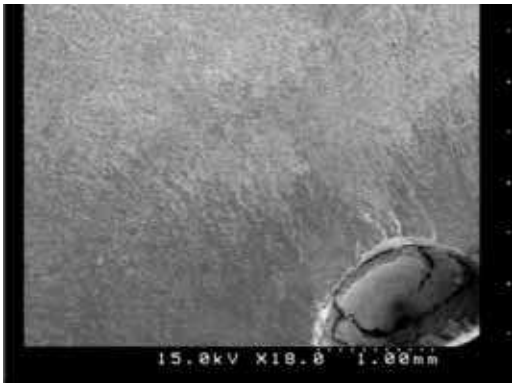

Fig. 18. Pitting deep shape

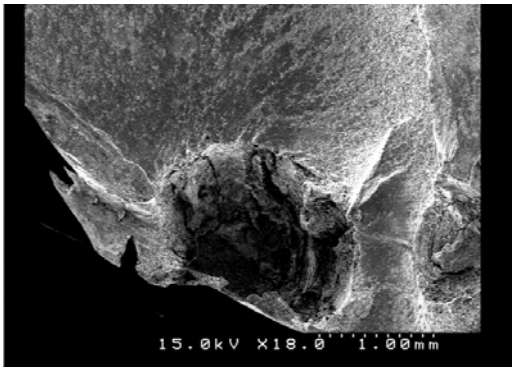

Fig. 19. Pitting deep shape

3.2 Fatigue initial point

In this section, the standard of material specimen is based on JIS G4303, 36 pieces specimen have been prepared for test and separated 4 groups, each group include 3 sets and 1 set include 3 pieces. Firstly, the acceleration pitting corrosion test has been carried out for all sampling pieces. After pitting corrosion, that be separated A, B, C and D group based on the post treatment condition. A group is without post treatment; B group is with solution treatment; C group is with preheated 1400℃ for metal coating and D group is preheated 200℃ for metal coating. The metal coating surface had been machined two sets among and other one set without machined for C and D group. The effects of the morphology and matrix structure on the fatigue process as well as fatigue life were examined through metallurgical graphic and fracture graphic observation. The metallurgical graphs of the fatigue fracture surfaces were studied by SEM and are shown in Figures 20 to Figure 23.

Under all test conditions, Figure 20 the crack initiation of Group A, was found to occur at the cavity inside the pitting deep; Figure 21, the crack initiation of Group B, the diameter of pitting deep have clearly increased from 0.1 mm to 0.5 or 1.0mm after solution treatment, and cannot find the fatigue prorogation from the fracture surface. So, the fatigue life cycles

had obviously decreased to compare between Table 4 and Table 5; Figure 22 6, the crack initiation of Group C, the microstructure of initiation point have different change with Group A due to the preheated process and can be found to occur at the fracture in the boundary; Figure 23, the crack initiation of Group D, the microstructure of initiation point have cleavage and fracture phenomenon. The tests without the metal surface, cannot find the fatigue initiation point and the fracture point in the near middle of surface, and the fatigue life cycle longer than other specimen.

The observations indicated that the fatigue life is not influenced in significant way by the mechanisms of interaction between dislocations and precipitates. It has been reported that at room temperature the fatigue life is influenced by the deformation mechanism. We believe that in the present work, which has been carried out at elevated temperature and under laboratory atmosphere, the fatigue life is essentially determined by the cracks initiated at the specimen surface as a result of intercrystal line oxidation. This view is supported by the observations, which are reported in Figure.

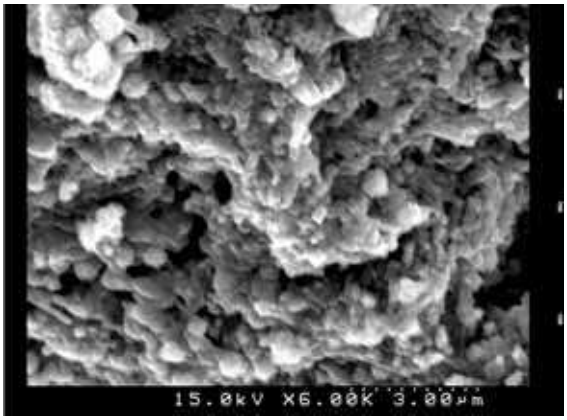

Fig. 20. Fatigue initial point of specimen (Group A)

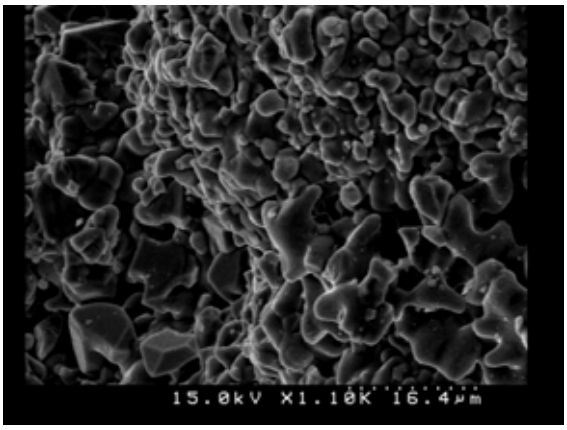

Fig. 21. Fatigue initial point of specimen (Group C)

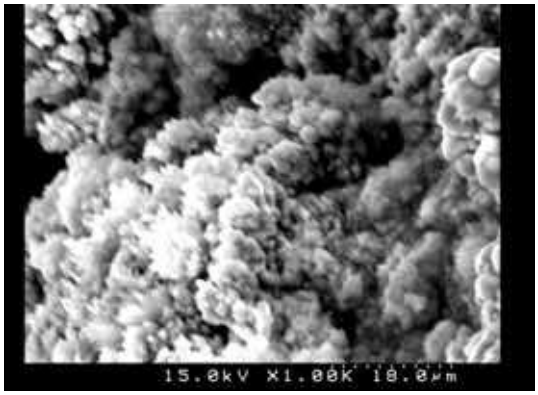

Fig. 22. Fatigue initial point of specimen (Group B)

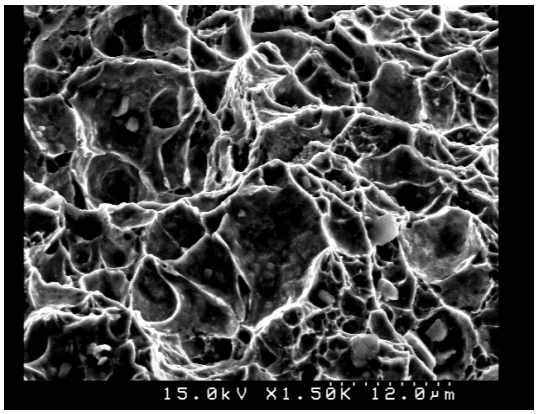

Fig. 23. Fatigue initial point of specimen (Group D)

3.3 Fatigue fracture mechanism observed by SEM

From the electron fractograhpy of the test specimen, there appears many different kinds of characteristic fatigue fracture features, which encompass the fatigue lines, the fatigue beach marks, the fatigue stair line, the critical crack length and the fracture area, etc.

3.3.1 Fatigue lines

In the fatigue crack propagation process, the fatigue lines appear along and in front of the trajectory of macroscopic plastic deformation at different instant, as shown in Figure 24. Usually, the normal direction of these fatigue lines is referred to as the direction of fatigue crack propagation.

3.3.2 Fatigue beach marks

Beach marks are similar to the fatigue lines that occur before fatigue crack and along the route of plastic deformation traced, as shown in Figure 25. Usually, their normal direction

approximately aims at the direction of the fatigue crack propagating. The number and the thickness of beach marks can be considered as the basis to measure fatigue endurance.

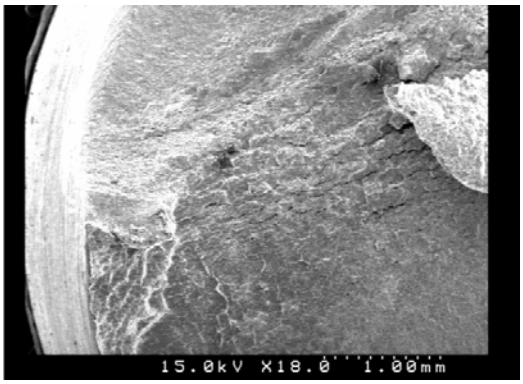

Fig. 24. Fatigue lines in fatigue fracture surface

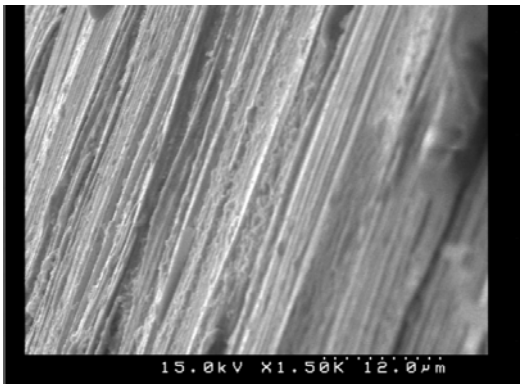

Fig. 25. Beach marks in initial fatigue stage

3.3.3 Fatigue stair lines

In various situations of fatigue failures, the fatigue stair line is one of the main characteristics of fatigue fracture. The fatigue stair lines can be often detected in the zone of obvious bright-gloomy band or curves, as shown in Figure 26. They are resulted from the merging or intersection of different fatigue crack propagation generated at different time and origins. Generally the direction of fatigue stair lines is normal to the direction of fatigue crack propagation. The direction and the density of the fatigue stair lines are the characteristic parameters used to identify the locations of fatigue origin sources.

3.3.4 Critical crack length

Critical (fatigue) crack length means the limit length of origin crack at which the fatigue crack propagation can occur. Beyond the critical crack length of origin crack source, it represents that the fracture occurs abruptly. Such critical fatigue crack length can be seen in Figure 27.

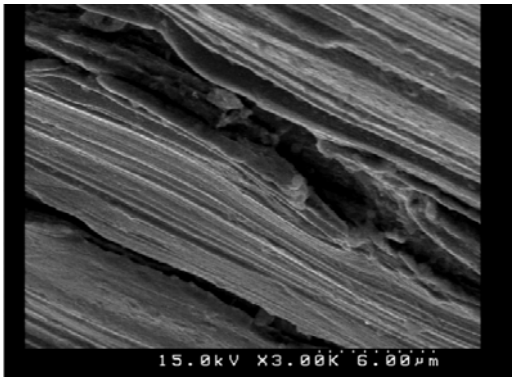

Fig. 26. Fatigue stair lines

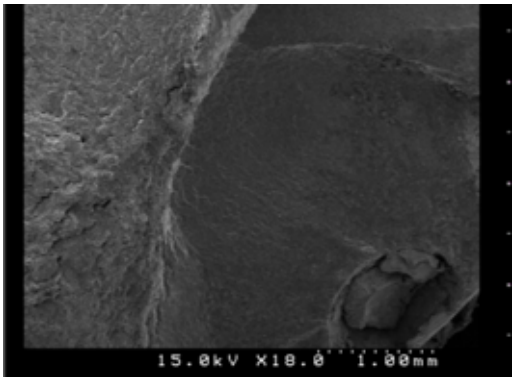

Fig. 27. Critical crack length

3.3.5 Fracture area

In the instantaneous fracture zone or referred to as the fracture area, it can be seen some crystalline patterns like river stream and tongue as shown in Figure 28 and Figure 29.

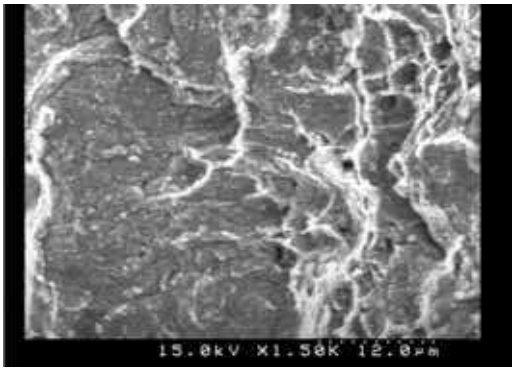

Fig. 28. Fracture area with river stream pattern

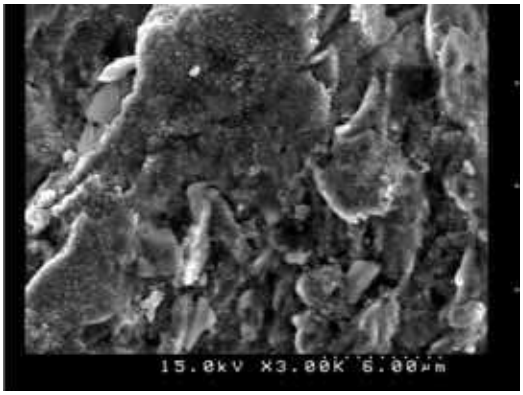

Fig. 29. Fracture area with tongue pattern

3.3.6 Transgranular and intergranular fracture

In the fracture area, fractures can be categorized as transgranular and intergranular fracture based on the fracture path related to the crystalline grain structure. Transgranular fracture may be ductile or brittle depending on the amount of grain deformation as shown in Figure 30. While intergranular fracture is only pertaining to a brittle one, since the separation of grains is usually due to the presence of brittle interface, as shown in Figure 31.

4. Pitting corroding rate

The grey systems are the systems that lack information, such as architecture, parameters, operation mechanism and system behavior, for example, for estimating the tendency of Typhoon landing in Taiwan [8]. There are a number of factors that affect the pitting corrosion rate of stainless alloy that include [a, b, c… and x] as previously mentioned.

The grey correlation analysis explains uncertain correlations between one main factor and all other factors in a given system. The grey correlation analysis method is based on the clustering approach in which the time factor is during the experiment period.

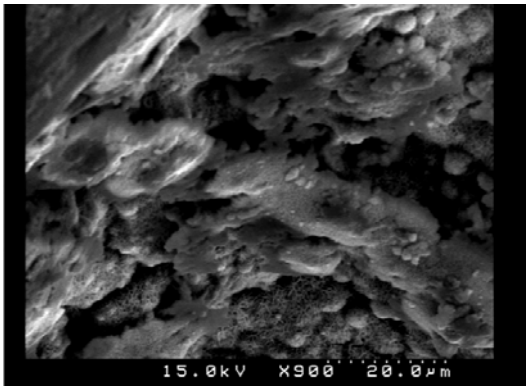

Fig. 30. Transgranular fracture at interior pitting deep

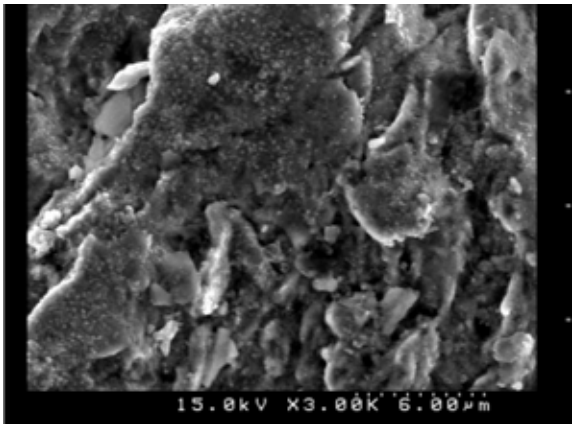

Fig. 31. Intergranular fracture in the fracture area

4.1 Material and experiment procedure

For this test, stainless SUS 630 was used and test specimen with a size of 50(L)*25(B)*5(t) mm. The Chemical property is shown as in Table 3.1 and the mechanical property is as shown in Table 3.2 for the SUS 630. All specimens were carried out the pitting corrosion test separated for the short term test (acceleration pitting corrosion test) and for long term test (environmental test). The acceleration pitting corrosion test was separated six (6) cases test and the environmental test was separated the static test and dynamic test.

The size of test period relates to size and development trend of the corroding rate. The test period of three chlorine iron solution is 72 hours according to the standard, this test, in order to further understand and corrode the relation with test period, and divided into 24, 48, 72 and 96 hours to wait for four cycles.

This test is divided into six (6) schemes, is mainly for the same test temperature, different pH value, such as Case 1, Case3 and Case 4; Another the same experimental pH value, different test temperature, such as Case 5 and Case 6. Case 2 utilizes Case 1 to finish the solution of the test, because the thickness of its chlorine ion is in order to reduce, repeat another test; it is shown in Table 1 and in detail picture as following specimen picture.

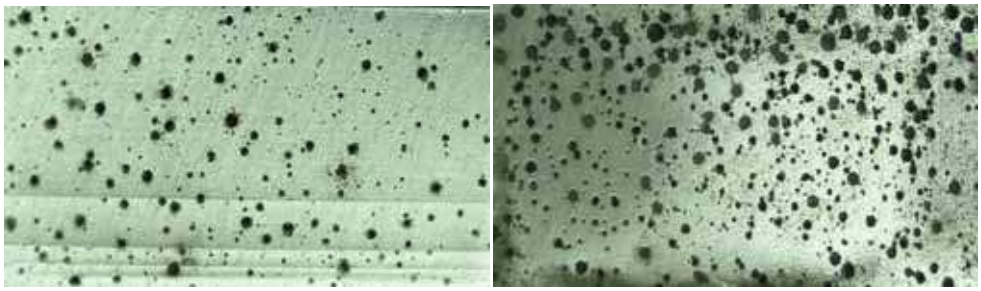

Specimen (I) Specimen (II)

Fig. 32. Specimen Picture

Material			SUS630									
Sample size			50mm*25mm*5mm									
CASE	1		2		3		4		5		6	
Test date	2002/2/14		2002/2/27		2002/3/25		2002/5/07		2002/07/02		2002/07/02	
Test temperature	25 ℃		22 ℃		25 ℃		25 ℃		32 ℃		26℃	
PH value	1.3		1.2		1.5		1.4		0.8		0.8	
sample groups	A	B	A	B	A	B	A	B	A	B	A	B
Test period	Specimen No.											
24 Hour	1A1	1B1	2A1	2B1	3A1	3B1	4A1	4B1	5A1	5B1	6A1	6B1
48 Hour	1A2	1B2	2A2	2B2	3A2	3B2	4A2	4B2	5A2	5B2	6A2	6B2
72 Hour	1A3	1B3	2A3	2B3	3A3	3B3	4A3	4B3	5A3	5B3	6A3	6B3
96 Hour	1A4	1B4	2A4	2B4	3A4	3B4	4A4	4B4	5A4	5B4	6A4	6B4

Table 1. Testing procedure

Measuring the pitting depth from experiment specimen, it note down ten(10) pitting deep relatively, asks its average, its unit is mm. and then called the corroding rate with the average divided by test period, its unit is mm/h, and about 10^6 times of the standard unit. The result record is shown as the Table 2.

Specimen No.	1A1	1A2	1A3	1A4	1B1	1B2	1B3	1B4
Average	0.352	0.509	1.116	0.945	0.48	0.762	1.04	0.997
Rate of Corrosion	0.0146667	0.0106042	0.0155000	0.0098438	0.0200000	0.0158750	0.0144444	0.0103854
Specimen No.	2A1	2A2	2A3	2A4	2B1	2B2	2B3	2B4
Average	0.00	0.678	0.00	0.785	0.38	0.518	0.55	0.35
Rate of Corrosion	0.0000000	0.0141250	0.0000000	0.0081771	0.0158333	0.0107917	0.0076389	0.0036458
Specimen No.	3A1	3A2	3A3	3A4	3B1	3B2	3B3	3B4
Average	0.399	0.725	0.643	0.763	0.545	0.776	1.024	0.779
Rate of Corrosion	0.0166250	0.0151042	0.0089306	0.0079479	0.0227083	0.0161667	0.0142222	0.0081146
Specimen No.	4A1	4A2	4A3	4A4	4B1	4B2	4B3	4B4
Average	0.441	0.684	0.774	0.908	0.555	0.549	1.025	1.09
Rate of Corrosion	0.0183750	0.0142500	0.0107500	0.0094583	0.0231250	0.0114375	0.0142361	0.0113542
Specimen No.	5A1	5A2	5A3	5A4	5B1	5B2	5B3	5B4
Average	0.654	0.567	0.919	0.934	0.665	1.15	0.91	1.228
Rate of Corrosion	0.0272500	0.0118125	0.0127639	0.0097292	0.0277083	0.0239583	0.0126389	0.0127917
Specimen No.	6A1	6A2	6A3	6A4	6B1	6B2	6B3	6B4
Average	0.384	0.503	0.675	0.702	0.52	0.69	0.736	0.798
Rate of Corrosion	0.0160000	0.0104792	0.0093750	0.0073125	0.0216667	0.0143750	0.0102222	0.0083125

Table 2. Pitting depth (unit mm) and corrode Rate (Unit mm/h)

Environmental test, its purpose in real environment, service life when used for and estimated and moved forward the axle department actually mainly, the two sets have been put in the sea side (Dynamic Test) at Keelung shipyard (China Ship Building Corporation) since May 2004 and four other sets have been put in plastic barrel with sea water (Static Test) in room since August 2004. The average temperature of sea water is around 25°C and

the pH value is about 7.2 for this test condition. All test pieces were retrieved monthly and the depth of pitting corrosion were measured and recorded accordingly.

The result record is shown as the Table 3 for the dynamic experiment, its unit is 1/100 mm, and the static experiment record is as shown the Table 4. If the unit was selected to mm/100/day, the Table 3 will be changed to Table 5 and Table 4 also changed to Table 6.

Specimen No.	Jun	Jul	Aug	Sept	Oct	Nov	Dec
SP1	37.5	70	100	125	135	140	147
SP2	36.5	65	80	98	110	125	137
Average	37	67.5	90	111.5	122.5	132.5	142
Specimen No.	Jan	Feb	Mar	Apr	May	Jun	Jul
SP1	152	152	153	154	154.5	155	155.5
SP2	148	151.5	152.5	153	153.5	154	154.5
Average	150	151.75	152.75	153.5	154	154.5	155

Table 3. The result of pitting corrosion depth of dynamic experiment (unit: 1/100mm)

Specimen No.	Sept	Oct	Nov	Dec	Jan	Feb
1SA	35	68	85	98	119	120
2SA	34.5	65	89	96	108	114
3SA	33.5	64	88	97	110	111
4SA	33	60	82	95	103	116
AVG	34	64.25	86	96.5	110	115.25
Specimen No.	Mar	Apr	May	Jun	Jul	
1SA	123	124	125	126	126.5	
2SA	118	120	122	123	123.5	
3SA	114	115.5	117	118	118.5	
4SA	120.5	122.5	123.5	125	125	
AVG	118.875	120.5	121.875	123	123.375	

Table 4. The result of pitting corrosion depth of static experiment (unit: 1/100mm)

Specimen No.	Jun	Jul	Aug	Sept	Oct	Nov	Dec
SP1	1.2500	1.1667	1.1111	1.0417	0.9000	0.7778	0.7000
SP2	1.2167	1.0833	0.8889	0.8167	0.7333	0.6944	0.6524
Average	1.2333	1.1250	1.0000	0.9292	0.8167	0.7361	0.6762
Specimen No.	Jan	Feb	Mar	Apr	May	Jun	Jul
SP1	0.6333	0.5630	0.5100	0.4667	0.4292	0.3974	0.3702
SP2	0.6167	0.5611	0.5083	0.4636	0.4264	0.3949	0.3679
Average	0.6250	0.5620	0.5092	0.4652	0.4278	0.3962	0.3690

Table 5. The result pitting corrosion rate of dynamic experiment (unit. mm/100/day)

Specimen No.	Sept	Oct	Nov	Dec	Jan	Feb
1SA	1.1667	1.1333	0.9444	0.8167	0.7933	0.6667
2SA	1.1500	1.0833	0.9889	0.8000	0.7200	0.6333
3SA	1.1167	1.0667	0.9778	0.8083	0.7333	0.6167
4SA	1.1000	1.0000	0.9111	0.7917	0.6867	0.6444
AVG	1.1333	1.0708	0.9556	0.8042	0.7333	0.6403

Specimen No.	Mar	Apr	May	Jun	Jul	
1SA	0.5857	0.5167	0.4630	0.4200	0.3833	
2SA	0.5619	0.5000	0.4519	0.4100	0.3742	
3SA	0.5429	0.4813	0.4333	0.3933	0.3591	
4SA	0.5738	0.5104	0.4574	0.4167	0.3788	
AVG	0.5661	0.5021	0.4514	0.4100	0.3739	

Table 6. The result pitting corrosion rate of static experiment (unit. mm/100/day)

4.2 Influence factor of corroding rate

According to measured data of pitting deep depth, utilizing the analytical method, can be estimated the distribution. Normal distribution can be regarded as the probability distribution of the corroding rate of stainless steel for pitting corrosion.

T-test is most commonly applied when the test statistic would follow a normal distribution if the value of a scaling term in the test statistic were known. The *t*-distribution is symmetric and bell-shaped, like the normal distribution, but has heavier tails, meaning that it is more prone to producing values that fall far from its mean. Using the Table 2, the upper and lower limit will be calculated by the t-test and t-distribution table shown as Table 7.

CASE 1						
Probability	0.5	0.95	0.99	0.5	0.95	0.99
t value	0.765	3.182	5.841	0.765	3.182	5.841
Lower Limit	0.01156615	0.00813025	0.00435033	0.01257010	0.00433614	-0.00472223
Upper Limit	0.01374113	0.01717703	0.02095695	0.01778232	0.02601628	0.03507466
CASE 2						
Lower Limit	0.00294363	-0.0053717	-0.0145197	0.00752982	0.00137642	-0.00539307
Upper Limit	0.00820741	0.01652281	0.02567078	0.01142503	0.01757843	0.02434793
CASE 3						
Lower Limit	0.01048792	0.00523060	-0.00055312	0.01256486	0.00391395	-0.00560312
Upper Limit	0.01381589	0.01907321	0.02485692	0.01804103	0.02669194	0.03620902
CASE 4						
Lower Limit	0.01168016	0.00685193	0.00154028	0.01252271	0.00457512	-0.00416820
Upper Limit	0.01473650	0.01956473	0.02487638	0.01755367	0.02550126	0.03424459
CASE 5						
Lower Limit	0.01232570	0.00264765	-0.0079994	0.01654468	0.00792052	-0.00156712
Upper Limit	0.01845207	0.02813012	0.03877718	0.02200392	0.03062808	0.04011573
CASE 6						
Lower Limit	0.01232570	0.00264765	-0.0079994	0.01654468	0.00792052	-0.00156712
Upper Limit	0.01845207	0.02813012	0.03877718	0.02200392	0.03062808	0.04011573

Table 7. Pitting deep upper and lower limits (unit mm) of depth

F-test is any statistical in which the test static has an F-distribution under the null hypothesis. It is most often used when comparing statistical models that have been fit to a data set, in order to identify the model that best fits the population from which the data were sampled. Exact *F-tests* mainly arise when the models have been fit to the data using least squares.

The hypotheses that the means of several normally distributed populations, all having the same standard deviation, are equal. This is perhaps the best-known F-test, and plays an important role in the analysis of variance (ANOVA).

In statics, analysis of variance is a collection of statistical models, and their associated procedures, in which the observed variance in a particular variable is partitioned into components attributable to different sources of variation. In its simplest form ANOVA provides a statistical test of whether or not the means of several groups are all equal, and therefore generalizes-test to more than two groups.

For a defect-free material, pitting corrosion is caused by the chemistry that may contain aggressive chemical species such as chloride. Chloride is particularly damaging to the passive film oxide so pitting can initiate at oxide breaks. The influence factors of pitting corrosion for stainless steel were complex, for example, material defect, solution pH value and temperature etc.

4.2.1 The corrodes rate between pitting depth and material defect

a. Under the conditions of 95% confidence interval, its upper and lower limit value are 0.00989783 and -0.00485264 for Case 1, 0.01245305 and -0.00464923 for Case 2, 0.01151913 and -0.00521705 for Case 3, 0.0095169 and -0.00585718 for Case 4, 0.01460108 and -0.00683025 for Case 5, 0.00966449 and - 0.00395963 for Case 6. Based on the above-mentioned value, the intersection of extreme value and it's including 0, According to the t-test principle, there is no obvious relation between corroded rate and material defect.
b. Using the ANOVA methods calculation and F value to assay, the calculated F value is less than the critical value of F value. So, there is no obvious relation between corroded rate and material defect.

4.2.2 The corrodes rate between pitting depth and pH value of solution

a. Under the conditions of 95% confidence interval, its upper and lower limit are 0.0056934 and -0.00468993 for Case 1 and Case 3 Group A, and 0.00999922 and -0.00974575 for Case 1 and Case 3 Group B, Based on the above-mentioned value, the intersection of extreme value and it's including 0, According to the t-test principle, there is no obvious relation between corroded rate and pH value.
b. Using the ANOVA methods calculation and F value to assay, the calculated F value is less than the critical value of F value. So, there is no obvious relation between corroded rate and pH value.

4.2.4 The corrodes rate between pitting depth and solution temperature

a. Under the conditions of 95% confidence interval, its upper and lower limit are 0.01341501 and -0.00468993 for Case 5 and Case 6 Group A, and 0.01476674 and -0.00350632 for Case 5 and Case 6 Group B, Based on the above-mentioned value, the intersection of extreme value and it's including 0, According to the t-test principle, there is no obvious relation between corroded rate and temperature.
b. Using the ANOVA methods calculation and F value to assay, the calculated F value is less than the critical value of F value. So, there is not an obvious relation between corroded rate and temperature.

4.3 Corroding rate

Theoretically, a local cell that leads to the initiation of a pit can be caused by an abnormal anodic site surrounded by normal surface, which acts as a cathode, or by the presence of an abnormal catholic site surrounded by a normal surface in which a pit will have disappeared due to corrosion. The corroding rate was calculated by the grey theory method and regression method and the result was shown as Figure 33 to Figure 38 using the environmental test data.

The precision of the prediction is around 96.44% and error rate is about 3.56% on average with the grey predication for dynamic test; the precision of the prediction is around 96.97% and error rate is about 3.03% on average with the grey predication for static test. Therefore, the grey model GM (1,1) is an acceptable method for the prediction of the Pitting corrosion depth and rate.

The corrosion depth and rate precision of the prediction is individually around 89.84% and 98.43% and error rate is about 10.16% and 1.57% on average with the regression predication for dynamic test; the corrosion depth and rate precision of the prediction is separately around 89.47% and 97.91%and error rate is about 10.53% and 2.09%on average with the regression predication for static test. Therefore, the regression method is an acceptable method for the prediction of the pitting corrosion rate, and the prediction method should be explored besides other statistics analysis method for the pitting corrosion depth.

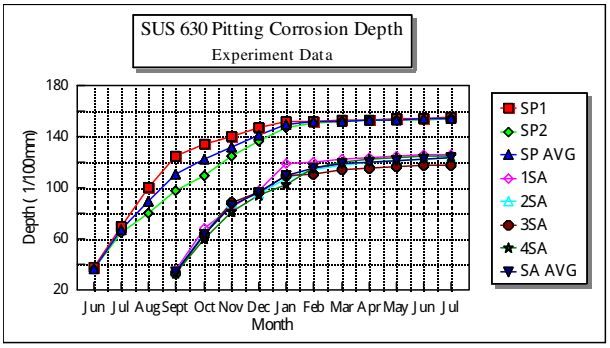

Fig. 33. Pitting corrosion depth of dynamic experiment and static experiment

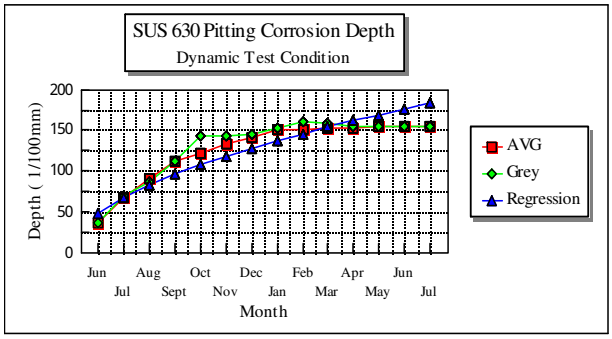

Fig. 34. Pitting corrosion depth of dynamic experiment with predict the curve graph by Grey and Regression

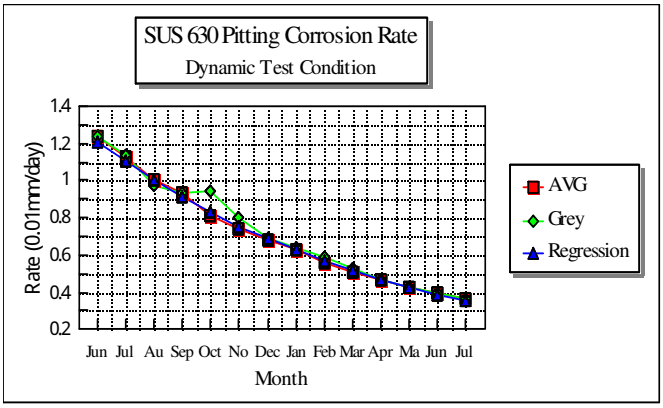

Fig. 35. Pitting corrosion depth of static experiment with predict the curve graph by Grey and Regression

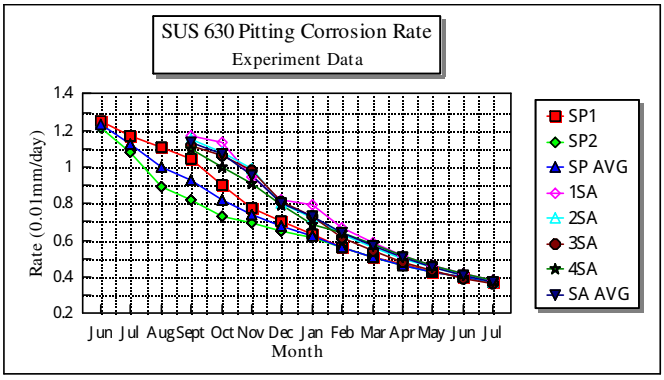

Fig. 36. Pitting corrosion ratio of dynamic experiment with predict the curve graph

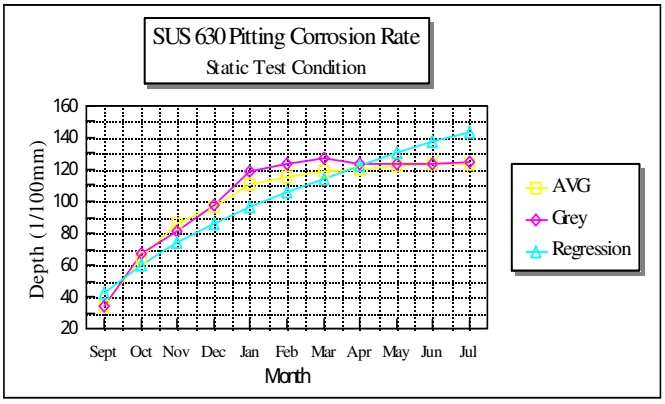

Fig. 37. Pitting corrosion rate of dynamic experiment with predict the curve graph by Grey and Regression

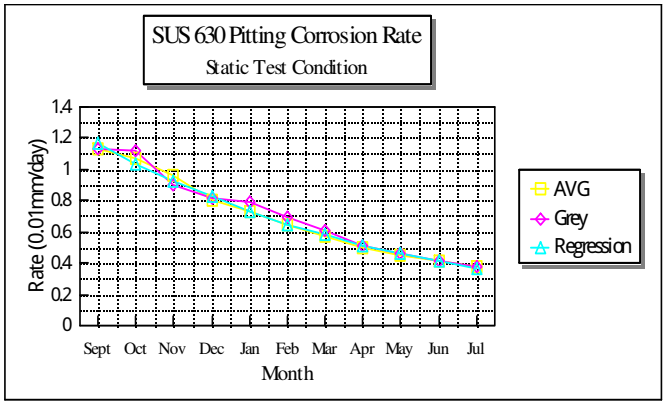

Fig. 38. Pitting corrosion rate of static experiment with predict the curve graph by Grey and Regression

5. Pitting corrosion fatigue life

As the condition of most pitting corrosion occurring on the surface of stainless steel shafts, when they are operating in fluid of neutral-to-acid solution, which especially containing chloride or chloride ions, there constitute multiple points of stress concentration on the shaft surface . The mechanism of multiorigin fatigue fracture may be more complicated than that of the above mentioned single point stress concentration condition.

5.1 Fatigue

In material science fatigue is the progressive and localized structural damage that occurs when a material is subjected to cyclic loading. The nominal maximum stress values are less than the ultimate tensile stress limit, and may be below the yield stress limit of the material.

A fatigue crack often starts at some point of stress concentration. This point of origin of the failure can be seen on the failed material as a smooth, flat, semicircular or elliptical region, often referred to as the nucleus. Surrounding the nucleus is a burnished zone with ribbed markings. This smooth zone is produced by the crack propagation relatively slowly through the material and the resulting fractured surfaces rubbing together during the alternating stressing of the component [1]. When the component has become so weakened by the crack that it is no longer able to carry the load, the final, abrupt fracture occurs, which shows a typically crystalline appearance.

Fatigue occurs when a material is subjected to be repeated loading and unloading. If the loads are above a certain threshold, microscopic cracks will begin to form at the surface. Eventually a crack will reach a critical size, and the structure will suddenly fracture. The shape of the structure will significantly affect the fatigue life; square deeps or sharp corners will lead to elevated local stresses where fatigue cracks can initiate. Round deeps and smooth transitions or fillets are therefore important to increase the fatigue strength of the structure.

According to the observation ways of a metal fracture, the fracture can be categorized into macroscopic and microscopic features. Marcroscopic fracture can be observed or inspected

by either naked eyes or a magnifying glass on the surface of the metal or the fracture surface. While the microscopic fracture can be observed only by a optical microscope or a scanning electron microscope (SEM). Owing to the enlarging area and depth is not so extensive by a optical microscope, therefore a SEM is used in this study. On the contrary, SEM can observe a broad range and deeper depth on the fracture surface. Through microscopic fracture surface observation, the crack propagation process and material intrinsic crystalline structure can be identified.

5.2 Fatigue life

The fatigue life time depends on several factors, where the most important one sere the manufacturing, the material properties, and the loading conditions, which are all more or less random. Both material properties and dynamical load process are important for fatigue evaluation, and should in more realistic cases be modeled as random phenomena.

Since the well-known work of Wöhler in Germany starting in the 1850's, engineers have employed curves of stress versus cycles to fatigue failure, which are often called S-N curves (stress-number of cycles) or Wöhler's curve.The basis of the stress-life method is the Wöhler S-N curve, that is a plot of alternating stress, S, versus cycles to failure, N. The data which results from these tests can be plotted on a curve of stress versus number of cycles to failure. This curve shows the scatter of the data taken for this simplest of fatigue tests.

ASTM defines fatigue life (N), as the number of stress cycles of a specified character that a specimen sustains before failure of a specified nature occurs. Fatigue life is the number of loading cycles of a specified character that a given specimen sustains before failure of a specified nature occurs. When analyzing the fatigue life for the structures, the level crossings have been used for a long time. However, better life predictions are obtained when using a cycle counting method, which is a rule for pairing local minima and maxima to equivalent load cycles. Fatigue damage is computed by damage accumulation hypothesis which is illustrated as Palmgren-Miner rule. This rule is used to obtain an estimate of the structural fatigue life.

In high-cycle fatigue situations, materials performance is commonly characterized by an S-N curve, also known as a wdeep curve. This is a graph of the magnitude of a cyclic stress (S) against the logarithmic scale of cycles to failure (N).

S-N curves are derived from tests on samples of the material to be characterized where a regular sinusoidal stress is applied by a testing machine which also counts the number of cycles to failure. This process is sometimes known as coupon testing. Each coupon test generates a point on the plot though in some cases there is a run out where the time to failure exceeds that available for the test. Analysis of fatigue data requires techniques from statistic, especially survival analysis and linear regression.

5.3 S-N curve with rotating bending test

5.3.1 Fatigue rotating bending test

For this rotating bending testing method followed JIS Z 2247-1978, the material is stainless SUS 630 and the test pieces standard is symbol 1-10 of class 1, and the speed of loading repetition is 2400 rpm. The value obtained by diving the bending moment at a cross section

generating the maximum stress by modulus of section shall be used as the nominal stress. The S-N curve will be drawn by plotting the values of stress amplitude as ordinate and the number of stress cycles. Configurations of the test machine and the specimen used in the study are shown as Figure 39 and Figure 40 respectively.

Fig. 39. Rotating bending fatigue test machine

Fig. 40. Specimens for fatigue test under rotating bending load

5.3.2 Fatigue life estimation

In this test, the number of cyclic stress reversals with constant amplitudes of 350 N/mm², 400 N/mm², 450 N/mm², 500 N/mm², 550 N/mm²and 600 N/mm², respectively, induced in the specimens is counted. In addition, the test for that on uncorroded specimens is also carried out. Hanging equivalent weight on the test specimen and rotating under the revolution speed of 2400 rpm attain these specified stress amplitudes.

Due to the yield stress around 725 N/mm²and maximum stress amplitude 600 N/mm² in this fatigue test, therefore, the fatigue life should be estimated with statistic method for over 600 N/mm² stress. According to the eempirical rule, the estimated theory will be selected the Grey Model GM (1,1) and Curvilinear Regression same as Section 4.

Using the experimentation data as input, a computer program was used to obtain the results in Tables 5.1. The S-N curve showing the experimentation, grey predication and regress analysis for SUS 630 fatigue test sample are shown in Figure 41 to Figure 42.

Stress (N/mm²)	Experiment	Grey Predicate	Regress Analysis
750		26503	12417
700		42784	24998
650		70640	50327
600	153500	119415	101320
550	218500	206914	203984
500	247800	367913	410670
450	523300	672130	826782
400	1800000	1263187	1664520
350	5000000	5000000	3351095

Table 8. Experiment, Grey Predication and Regress Analysis value

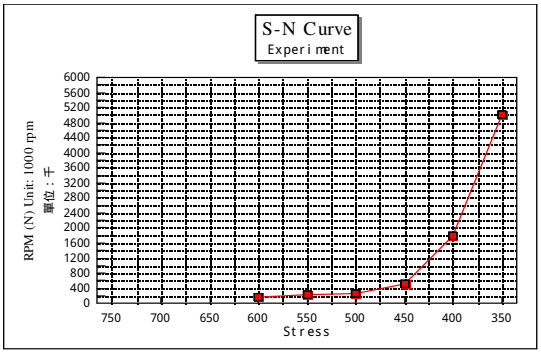

Fig. 41. S-N Curve with experiment

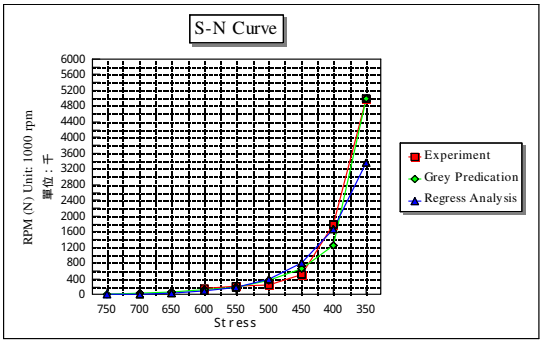

Fig. 42. S-N Curve with Experiment, Grey Predication and Regress Analysis

The precision of the prediction is around 98.31875 with the grey predication;, the precision of the prediction is around 97.54732 with the regress analysis. Therefore, the grey model GM (1,1) is an acceptable method for the prediction of the S-N curve.

The grey system theory has been used to deal with partially known and unknown data for stainless alloy. Traditional prediction usually employs the statistical method for large samples of data. According to the above-mentioned results, the grey system theory is also suitable for use to predict the S-N curve the scarcity of available data.

5.4 S-N curve under pitting corrosion condition

5.4.1 Ferric Chloride Test (FCT)

In order to accelerate the generation of SUS 630 shaft specimen with various extents pitting corrosion to facilitate the fatigue crack propagation study, the ferric chloride test (FCT) in accordance with the standard of JIS G 0578: 2000, is performed. Besides, the ferric chloride test can be used to evaluate the pitting resistance of stainless steels. At first, the test specimens were put in the ferric chloride solution with concentration 6% and carry out continuous immersion for 24hours, 48hours and 72hours respectively. Thus, three sets of specimen are prepared. They are specimen No. 3A1, 3A2, and 3A3 attained from 24h FCT; specimen No. 1A1, 1A2, and 1A3 from 48h FCT; and specimen No. 2A1, 2A2, and 2A3 from 24h FCT.

After the 24h, 48h and 72h immersion, the test specimens are taken out from the test solution. After removing the crusts generated by corrosion and a dial gauge measures washing and drying the specimens, the pitting depth at five representative points. The measured depths together with the average pitting depth are shown in Table 9.

	24 h FCT	48 h FCT	72h FCT
Specimen No.	3A1	1A1	2A1
Average depth (mm)	0.31	0.57	0.71
Specimen No.	3A2	1A2	2A2
Average depth (mm)	0.44	0.59	0.72
Specimen No.	3A3	1A3	2A3
Average depth (mm)	0.45	0.66	0.80

Table 9. Measured record and average pitting depth of test specimen

5.4.2 Fatigue life of pitting corrosion

The fatigue test was carried out with rotating bending test equipment under the number of cyclic stress reversals with constant amplitudes of 350 N/mm^2, 400 N/mm^2 and 450 N/mm^2, respectively, induced in the specimens is counted.

The fatigue life (N_f) can be divided into the number of cycles, (N_i) necessary to initiate a stage I micro crack, which has a size of the order of the grain size, and the number of cycles, (N_p) for crack propagation. Then a crack growth law relating the propagation rate of each microcrack to the applied plastic strain and crack length is derived metallographic observations. The third stage of fatigue damage, which leads to final fracture, is modeled as the coalescence of this population of microcracks which are nucleated and which propagate continuously. The measurement data for the fatigue test belong to the N_p in Table 10 to Table 13.

24 Hours		
Specimen No.	Test stress range (N/mm²)	No. of cycles(cycles)
3A2	450	144200
3A1	400	155200
3A3	350	244100
48 Hours		
Specimen No.	Test stress range (N/mm²)	No. of cycles(cycles)
1A2	450	103200
1A1	400	124100
1A3	350	151200
72 Hours		
Specimen No.	Test stress range (N/mm²)	No. of cycles (cycles)
2A2	450	64000
2A1	400	97600
2A3	350	123500

Table 10. Measurement data of the experiment (without any treatment)

24 Hours		
Specimen No.	Test stress range (N/mm²)	No. of cycles(cycles)
2B2	450	14700
2B1	400	32700
2B3	350	47800
48 Hours		
Specimen No.	Test stress range (N/mm²)	No. of cycles(cycles)
1B2	450	11700
1B1	400	18500
1B3	350	33200
72 Hours		
Specimen No.	Test stress range (N/mm²)	No. of cycles (cycles)
3B1	450	
3B2	400	20300
3B3	350	26900

Table 11. Measurement data of the experiment (with solution treatment)

24 Hours (coating surface with machined)		
Specimen No.	Test stress range (N/mm²)	No. of cycles(cycles)
2C2	450	14500
2C1	400	27400
2C3	350	63700
48 Hours (coating surface with machined)		
Specimen No.	Test stress range (N/mm²)	No. of cycles(cycles)
1C2	450	14100
1C1	400	27100
1C3	350	62700
72 Hours (coating surface without machined)		

Specimen No.	Test stress range (N/mm²)	No. of cycles (cycles)
3C2	450	78700
3C1	400	94300
3C3	350	142100

Table 12. Measurement data of the experiment (with metal coating treatment)

24 Hours (coating surface with machined)		
Specimen No.	Test stress range (N/mm²)	No. of cycles(cycles)
2D2	450	21600
2D1	400	38500
2D3	350	65900
48 Hours (coating surface with machined)		
Specimen No.	Test stress range (N/mm²)	No. of cycles(cycles)
1D2	450	13500
1D1	400	25100
1D3	350	27600
72 Hours (coating surface without machined)		
Specimen No.	Test stress range (N/mm²)	No. of cycles (cycles)
3D2	450	105400
3D1	400	134800
3D3	350	670000

Table 13. Measurement data of the experiment (with metal coating treatment)

5.4.3 Fatigue behavior of pitting corrosion

The test results of the number of cyclic stress reversals till fatigue fracture of the specimens are listed in Table 14. In Table 14, the fatigue lifetime ratio of pitting corrosion condition of the specimen is only about 12 - 27% of the fatigue time of uncorroded condition for the case of the working stress variation range 450 N/mm². the range of fatigue lifetime ratios even lower to 5.2 - 8.6 % and 2.5 - 4.8% for stress variation amplitudes 400 N/mm² and 350 N/mm² stress amplitude respectively.

Stress amplitude (N/mm²)	No. of cyclic stress reversals of specimen				Fatigue life ratio
	Uncorroded	24h FCT	48h FCT	72h FCT	
600	153500				
550	218500				
500	247800				
450	523300	144200	103200	64000	12 - 27 %
400	1800000	155200	124100	97600	5.2 - 8.6%
350	5000000	244100	151200	123500	2.5 - 4.8%

Table 14. Fatigue life test on specimens of uncorrod condition and pitting corrosion condition

6. Material constant

Failures occurring under condition of dynamic loading are called fatigue failures, presumably because up to the present it has been believed that these failures occur only

after a considerable period of service. Fatigue is said to account for at least 90 percent of all service failure due to a mechanical cause.

Fatigue results in a brittle-appearing fracture, with no gross deformation at the fracture. On a macroscopic the fracture surface is usually in line with the direction of the principal tensile stress.

A fatigue failure can usually be recognized from the appearance of the fracture surface, which shows a smooth region, due to the rubbing action caused by the crack propagation through the section; and a rough region, due to the member failing in a ductile manner caused by the cross section being no longer able to carry the load.

6.1 Fatigue crack propagation

Considerable research has gone into determining the laws of fatigue crack propagation for stage II growth. The crack propagation rate da/dN is found to follow an equation:

$$\frac{da}{dN} = C \cdot \sigma_a^m \cdot a^n \tag{1}$$

where

C: constant

σ_a : alternating stress

a: crack length

The most important advance in placing fatigue crack propagation into a useful engineering context is the realization of the fact that crack length versus cycles at a series of different stress levels could be expressed by a general plot of da/dN versus ΔK. da/dN is the slop of the crack growth curve at a given value of *a*, and ΔK is the range of the stress intensity factor, defined as

$$\begin{gathered} \Delta K = K_{\max} - K_{\min} \\ \Delta K = \sigma_{\max}\sqrt{\pi a} - \sigma_{\min}\sqrt{\pi a} = \sigma_r\sqrt{\pi a} \end{gathered} \tag{2}$$

Since the stress intensity factor is undefined in compressions, K_{min} is taken as zero if σ_{min} is compression.

Region II represents an essentially linear relationship between log da/aN and log ΔK

$$\frac{da}{dN} = C(\Delta K)^n \tag{3}$$

where:

$$\Delta K = \Delta\sigma(\pi a)^{\frac{1}{2}} Y \qquad \Delta K = A(a)^{\frac{1}{2}}$$

For this empirical relationship *n* is the slop of the curve and *A* is the value found by extending the straight line to $\Delta K = 1$ MPa $m^{1/2}$.

The equation (3) is often referred to as Paris's law. The equation provides an important link between fracture mechanics and fatigue.

Estimation the Fatigue crack propagation

If let the fatigue crack propagation for each cycle revolution is μ, then,

$$\mu = \frac{da}{dN} \tag{4}$$

or

$$dN = \frac{da}{\mu} \tag{5}$$

where:

a crack depth
N cycle revolution

First, measure the pitting deep depth and assume the depth is the crack beginning depth (a_0), then, measure the depth of the smooth area and assume the depth is the fatigue propagation depth (a_p), next, get the beginning depth plus the fatigue propagation depth and assume the depth is the critical depth (a_c). Finally, use the equation (6) and find the life cycle of the fatigue propagation (N_p).

$$N_p = \int_{a_0}^{a_c} \frac{da}{\mu} \tag{6}$$

where:

a_0 the depth of crack beginning propagation
a_c the critical depth

The crack propagation ratio is show in the formula (7) when the structure has been loaded with a stable alternating stress.

$$\begin{aligned} \frac{da}{dN} &= C_1 \Delta K^{n_1} \qquad 10^{-6} < \frac{da}{dN} < 10^{-4} \qquad (\text{mm / N}) \\ \frac{da}{dN} &= C_2 \left(\Delta K - \Delta K_{th}\right)^{n_2} \qquad 0 < \frac{da}{dN} < 10^{-6} \qquad (\text{mm / N}) \\ \frac{da}{dN} &= 0 \qquad \Delta K < \Delta K_{th} \end{aligned} \tag{7}$$

where:

C_i, n_i (i = 1,2…) material constant coefficient

The Paris formula can be deduced from the relations between the ratio of fatigue propagation and the crack depth as follows:

$$\frac{da}{dN} = C\left(\Delta K\right)^n \tag{8}$$

$$\Delta K = \Delta\sigma(\pi a)^{\frac{1}{2}} Y \tag{9}$$

where:

C, n material constant;
Y geometry factor;
Δσ the difference between maximum stress (σ_{max}) and minimum stress (σ_{min});
a crack depth

with the giving structure and the constant alternate load (Δσ), the equation (9) can be rewritten as follows:

$$\Delta K = A(a)^{\frac{1}{2}} \tag{10}$$

where:

$A = Y \cdot \pi^{\frac{1}{2}} \Delta\sigma = const$

$$\mu = \frac{da}{dN} = C(A\sqrt{a})^n = C_0 a^{\frac{n}{2}} \tag{11}$$

where:

$C_0 = CA^n$

$$N_p = \int_{a_0}^{a_c} \frac{da}{C_0 a^{n/2}} = \frac{2}{(2-n)C_0} a^{1-\frac{n}{2}} |_{a_0}^{a_c} = \frac{2}{(2-n)C_0} [a_c^{1-\frac{n}{2}} - a_0^{1-\frac{n}{2}}] \tag{12}$$

The constant C_0 and n can be decided with the following method, if, both sides of the equation (11) are taken with log function as follows:

$$\log\left(\frac{da}{dN}\right) = \log C_0 + (\frac{n}{2}) \log a \tag{13}$$

so,

The relation between $\log\left(\frac{da}{dN}\right)$ and $\log a$ is linear, the intercept is $\log C_0$; the slop is $\frac{n}{2}$,

Therefore, the corresponding value is $\left(\frac{da}{dN}\right)_i$ for the different crack depth (a_i), it varies according to the equation (13) and act as a go-between to all or division. The captioned formula can be derived as C_0 and $\frac{n}{2}$, and will be able to comply with equation (12), then N_p can be derived from equation (12).

6.2 Methodology

The Ferric Chloride Test (FCT) has been carried out same as the above 5.3.1 for the pitting corrosion and the fatigue tests are carried out for the sampling pieces; then, the

metallurgical graphics are taken through the Scanning Electron Microscope (SEM) for the fatigue fracture surface.

The fatigue test result data and measuring the initial crack and critical crack depth from the SEM graphic are shown in the Table 15, Table 16 and Table 17.

Specimen No.	Test stress	Fatigue revolution (rpm)	Initial crack depth (a_0)(mm)	Critical crack depth (a_c)(mm)
3A2	450	144200	0.78	4.15
3A1	400	155200	1.23	3.26
3A3	350	244100	1.07	4.85

Table 15. 24h FCT fatigue test data and measuring record

Specimen No.	Test stress	Fatigue revolution (rpm)	Initial crack depth (a_0)(mm)	Critical crack depth (a_c)(mm)
1A2	450	103200	1.20	4.47
1A1	400	124100	1.13	3.83
1A3	350	151200	1.53	4.13

Table 16. 48h FCT fatigue test data and measuring

Specimen No.	Test stress	Fatigue revolution (rpm)	Initial crack depth (a_0)(mm)	Critical crack depth (a_c)(mm)
2A2	450	64000	1.10	3.77
2A1	400	97600	0.70	2
2A3	350	123500	1.00	4.52

Table 17. 72h FCT fatigue test data and measuring record

6.3 Material constant

Figure 43 show the metallurgical graphics of the fatigue fracture surface with the SEM. The graphics allow to measure the initial crack depth (pitting deep depth) and to calculate the critical crack depth. The result is shown as Table 15 to Table 17.

	450 N/mm^2	400 N/mm^2	350 N/mm^2
A	797.60	708.98	620.36
K	704.425	786.30	620.36
C0	1.17E-6	1.08E-6	1.05E-6
C	1.72E-14	3.47E-15	4.40E-15
n	2.7	2.98	3.0
da/dN	8.39E-7	1.47E-6	1.16E-6

Table 18. SUS630 Material Constant and Fatigue Crack Propagation Constant

The fatigue crack propagation can be estimated using the data of Table 15 to Table 17 and the results that can be obtained as shown in Table 18. Table 18 gives the ranges of constant n

(2.7 to 3.0), constant (C 3.47E-15 to 1.72E-14) and da/dN (8.39E-7 to 1.47E-6). The tendency curves of the constant n, C and da/dN are shown in Figure 44 to Figure 46.

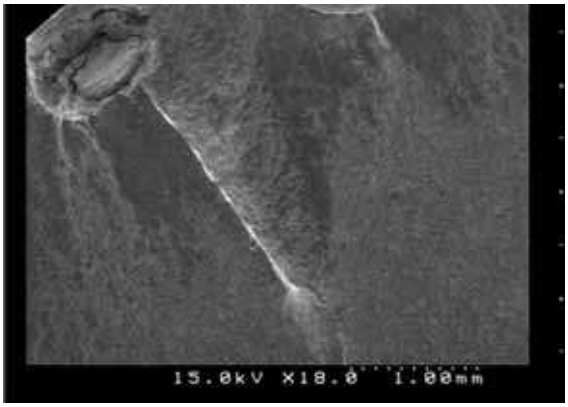

Fig. 43. Fatigue propagation area

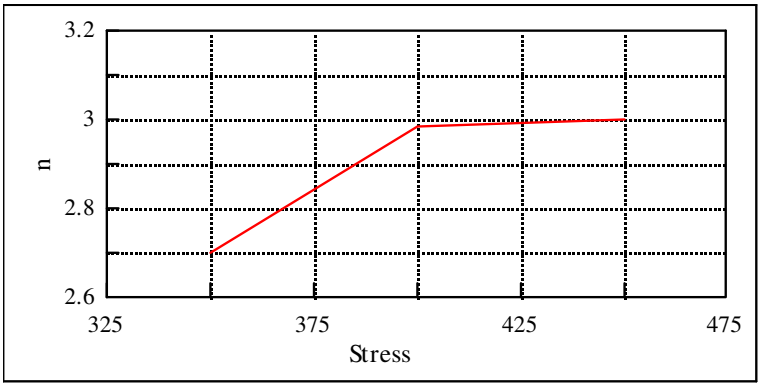

Fig. 44. n Tendency Curve

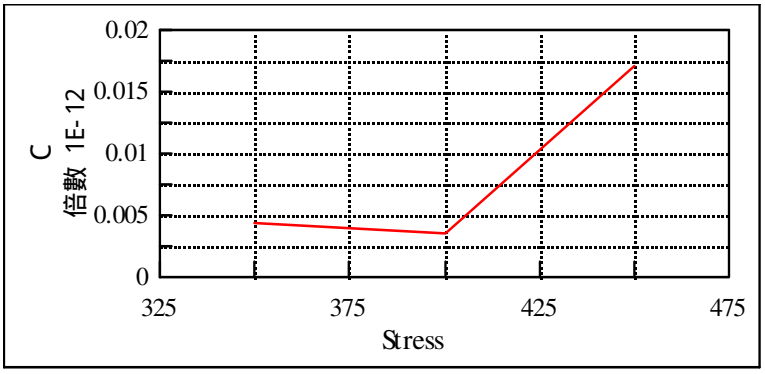

Fig. 45. C Tendency Curve

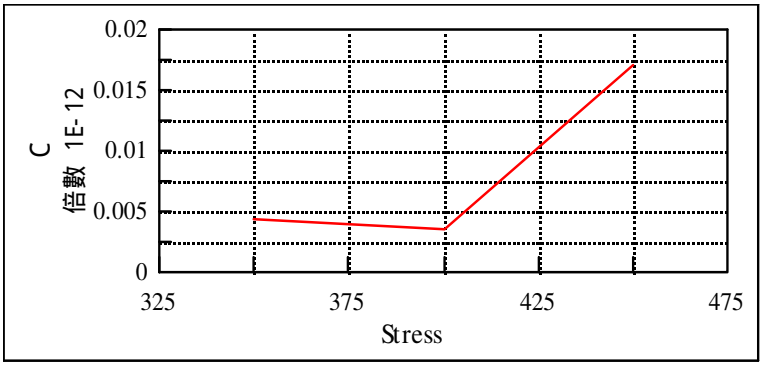

Fig. 46. da/dN Tendency Curve

7. Summery

Present knowledge about the relations between the microstructure changes and durability is still limited. This is the complex problem and it is necessary to deal with it as the separate question in the low-cycle fatigue durability estimation methodology. Material properties change in the low-cycle fatigue process, because most of the structural materials as steel for example are metallurgical unstable when they are cyclically deformed particularly at high temperature. Their dislocation structure changes determine the crack initiation in steel and their macroscopic behavior.

The fatigue lifetime of SUS 630 shaft under various extent of pitting corrosion condition is found to be in a range of only 2.5~27% of that of the uncorroded condition. These results are obtained by the ferric chloride test and rotating bending fatigue test on the SUS 630 shaft specimen. Apart from the feature of common fatigue fracture starting from a single point of stress concentration, i.e., forming initial stress nucleus, propagating ribbed markings and complete fracture zone, there existed much more sophisticated features on the fatigue fracture surfaces generated by multi points of stress concentration around the pitting deeps. Such as the fatigue lines, the fatigue beach marks, the fatigue stair lines, the critical crack length, the river stream pattern, tongue pattern and tree pattern in fracture area, transgranular and intergramular fractures, etc., have been detected and identified by using a SEM in the study.

Fatigue life showed difference depending on the matrix structure. The apparent difference of the fatigue life between the stress and the strain controlled cycling was well correlated in each material by means of cyclic stress-strain relationship. The grey system theory has been used to deal with partially known and unknown data for stainless alloy. Traditional prediction usually employs the statistical method for large samples of data. According to the above-mentioned results, the grey system theory is also suitable for use to predict the S-N curve the scarcity of available data.

Any of the three basic factors may cause fatigue failure list below. These are (1) a maximum tensile stress of sufficiently high value, (2) a large enough variation or fluctuation in the applied stress, and (3) a sufficiently large number of cycles of the applied stress. In addition, there are a host of other variables, such as stress concentration, corrosion, temperature,

overload, metallurgical structure, residual stresses, and combined stresses, which tend to alter the conditions of fatigue. Since we have not yet gained a complete understanding of what causes fatigue in metals, it will be necessary to discuss each of these factors from an essentially empirical standpoint. Due to the availability of a great mass of data, it would only to describe the highlights of the relationship between these factors and fatigue.

Constant n will be increased when the stress strength is increased. The rise ratio is rapid when the stress strength is less than the fatigue stress, the rise ratio is slow when the stress strength is bigger than the fatigue stress; Constant C will go down when the stress strength is less than the fatigue stress, constant C will go up when the stress strength is bigger than the fatigue stress; Constant da/dN will go up when the stress strength is less than the fatigue stress, The constant da/dN will be decreased when the stress strength is bigger than the fatigue stress. The fatigue strength is a breakpoint for the material constants n, C and da/dN of the fatigue fracture for the stainless SUS 630.

8. References

[1] Chin-Ming Hong Lon-Biou Li A Study of the Application of the Grey Correlation and the Analysis of Excellence Journal of Technology, Vol. 12 No. 1 1997 (in Chinese)

[2] Chang-Huang Chen A New Form of Grey Relational Coefficient Journal of Tung Nan Institute of Technology 2002

[3] Denny A. Jones Principles and Prevention of Corrosion Prentice Hall Inc. (1996)

[4] Der Norske Veritas Annual Report The New Risk Reality 2002

[5] Fong Yuan Ma ,Wei Hui. Wang A Study of the Relation between Economic Growth Rate and Shipping Industry Growth Rate Prediction and based on the Grey System Theory The conference of Cross-Strait for Navigating and Logistic 2004

[6] Fong Yuan Ma A Study of Tendency of Typhoon Landing in Taiwan of Using GM(1,1) Model The conference of Cross-Strait for Seamen 2004.

[7] Fong Yuan Ma and Wei Hui Wang, Fatigue crack propagation estimation of SUS 630 shaft based on fracture surface analysis under pitting corrosion condition, Material Science & Engineering A430, 2006, 1-8.

[8] Fong Yuan Ma and Wei Hui Wang, Prediction of pitting corrosion behavior for stainless SUS 630 based on grey system theory, Material Letters, 2006.

[9] Fong Yuan Ma ,Wei Hui. Wang *Estimating the Fatigue Life by Grey Theory for Propulsion Shaft of High Speed Craft* The 7th International Symposium on Marine Engineering conference 2005

[10] Fong Yuan Ma *Design Criterion Evolution of Shipboard Propulsion Shafting System Based on Classification Rules* The TEAM Conference 2005

[11] George E. Dieter, Mechanical Metallurgy, McGraw-Hill Book Company, 1988.

[12] G.S. Frankel, Pitting Corrosion Metals Handbook, Ohio State University 1994

[13] Japanese Standards Association, JIS Handbook, Ferrous Materials and Metallurgy I, 2002.

[14] J. L. Deng Basic of Grey System Theory Huazhong University Science and Technology Press, 2003 (in Chinese)

[15] Joseph F. Healey *Statistics: A tool for Social Research* Wadsworth Publishing Company 1995

[16] Jyh-Horng Wen and Yung-Fa Huang Application of Grey Prediction on Cellular Mobile Communication Systems IICM Vol. 3 No. 1 2000
[17] K. Enami, Y. Hagiwara, H. Mimura Assessment Method of Ductile and Brittle Fracture Initiation in High Strength Steels Journal of the Society of Naval Architects of Japan Vol. 195 2004
[18] M. Mohri & others A System Development in Predicating Fatigue Crack Paths and its Verification by Fatigue Tests Journal of the Society of Naval Architects of Japan Vol. 194 2003
[19] Petinov, S., Fatigue Analysis of Ship Structures, Backborne Publishing Company, 2003.
[20] P. Shi and S. Mahadevan Corrosion fatigue and multiple site damage reliability analysis International Journal of Fatigue June 2003.
[21] Ruey-Hsun Liang A Hybrid Grey System-Dynamic Programming Approach for Thermal Generating Unit Commitment Journal of Science and Technology Vol. 8 No. 1 1999
[22] SECIL ARIDURU Fatigue life calculation by rainflow cycle counting method 2004.
[23] Thomas Leonard, John S. J. Hsu *Bayesian Methods: An Analysis for Statisticians and Interdisciplinary Researcher* Cambridge University Press in 1999
[24] Walter A. Rosenkrantz *Introduction to Probability and Statistics for Scientists and Engineers* The Mcgraw-Hill Companies, Inc. 1995
[25] William Bolton, Engineering Materials 2, Newness ed, 1993

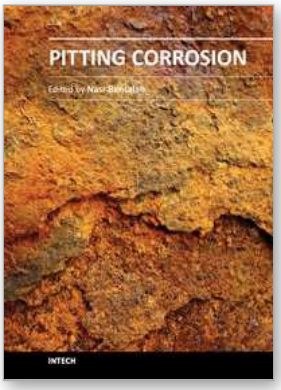

Pitting Corrosion

Edited by Prof. Nasr Bensalah

ISBN 978-953-51-0275-5
Hard cover, 178 pages
Publisher InTech
Published online 23, March, 2012
Published in print edition March, 2012

Taking into account that corrosion is costly and dangerous phenomenon, it becomes obvious that people engaged in the design and the maintenance of structures and equipment, should have a basic understanding of localized corrosion processes. The Editor hopes that this book will be helpful for researchers in conducting investigations in the field of localized corrosion, as well as for engineers encountering pitting and crevice corrosion, by providing some basic information concerning the causes, prevention, and control of pitting corrosion.

How to reference

In order to correctly reference this scholarly work, feel free to copy and paste the following:

Fong-Yuan Ma (2012). Corrosive Effects of Chlorides on Metals, Pitting Corrosion, Prof. Nasr Bensalah (Ed.), ISBN: 978-953-51-0275-5, InTech, Available from: http://www.intechopen.com/books/pitting-corrosion/corrosive-effects-of-chlorides-on-metals

INTECH
open science | open minds

InTech Europe
University Campus STeP Ri
Slavka Krautzeka 83/A
51000 Rijeka, Croatia
Phone: +385 (51) 770 447
Fax: +385 (51) 686 166
www.intechopen.com

InTech China
Unit 405, Office Block, Hotel Equatorial Shanghai
No.65, Yan An Road (West), Shanghai, 200040, China
中国上海市延安西路65号上海国际贵都大饭店办公楼405单元
Phone: +86-21-62489820
Fax: +86-21-62489821